ARMY RESEARCH LABORATORY

A One-Dimensional Atmospheric Boundary Layer Model: Comparison with Observations

Arnold Tunick

ARL-MR-484 September 2000

The findings in this report are not to be construed as an official Department of the Army position unless so designated by other authorized documents.

Citation of manufacturer's or trade names does not constitute an official endorsement or approval of the use thereof.

Destroy this report when it is no longer needed. Do not return it to the originator.

Army Research Laboratory

Adelphi, MD 20783-1197

ARL-MR-484 **September 2000**

A One-Dimensional Atmospheric Boundary Layer Model: Comparison with Observations

Arnold Tunick

Computational and Information Sciences Directorate

Abstract

This report examines details of a one-dimensional (1D) atmospheric boundary layer model to establish the proper functioning of its soil, plant, and atmospheric physics. To achieve this goal, I inspect, repair, and modify a computer program that scientists at the Hebrew University, Department of Soil and Water Sciences, gave to me years ago. The computer program was exercised to determine if the model results are stable when initial conditions are changed and to determine whether the results are sensible and generally consistent with observed data. To show this, I present a time series of the modeled surface energy budget and modeled profiles of boundary layer wind speed, potential temperature, and specific humidity for daytime (atmospherically unstable conditions) and for nighttime (atmospherically stable conditions). I compare these results, wherever practical, with observed meteorological data. From these results, I infer how well the transfers of momentum, heat, and moisture from one model layer to the next are characterized. I also present root mean square error and d values, where d is an index of agreement, to summarize the model results and comparison with observed data. From the results, I find that the 1D model is functioning properly in solving for many parameter relationships and is as reliable as the earlier models of this type in predicting the general features of boundary layer development.

Contents

1 Introduction **1**

2 Model Description **2**

3 Numerical Methods and Boundary Conditions **7**

4 Days 33 and 34 Observations **8**

5 Model Results **9**

6 Conclusion **15**

Acknowledgments **16**

References **17**

Appendix—Symbols and Definitions **19**

Distribution **21**

Report Documentation Page **25**

Figures

1 Sketch of geometry (i.e., vertical levels) of model 4

2 Modeled u and v components of wind speed and total wind, compared with observations 9

3 Modeled surface (θ_{sfc}) temperatures compared with earlier study and modeled 2-m ($\theta_{2\mathrm{m}}$) air temperatures compared with observations 11

4 Modeled surface energy budget compared with observations . . 11

5 Modeled height of planetary boundary layer compared with observations 11

6 Model boundary layer wind speed profiles compared with observations 12

7 Modeled potential temperature and specific humidity profiles compared with observations 13
8 Scatter plot comparisons of modeled results to observed data . 14

Tables

1 Boundary layer model parameters 3
2 Summary of model results in comparison with observed data . 10
3 Days 33 and 34 geostrophic wind data 12

1. Introduction

The atmospheric boundary layer is also called the friction layer. It extends from the earth's surface to the geostrophic wind (or gradient wind) level. Above this layer is the free atmosphere—where the frictional influence of the earth's surface is greatly diminished, allowing for an approximate balance between pressure gradient and Coriolis accelerations (Huschke, 1959). The daytime boundary layer is often observed to heights of 1 to 3 km above-ground level (agl), generating convective eddies (thermal updrafts and downdrafts) and relatively well-mixed profiles of wind speed, temperature, and moisture. In contrast, the nighttime boundary layer is characterized by a temperature inversion caused by a strong radiative cooling at the surface. The nighttime boundary layer can be at heights of 300 to 400 m agl. A low-level wind maximum or jet can sometimes develop in the nighttime boundary layer with faster, warmer air flow aloft, and slower, cooler air at the surface. This development of a low-level jet can promote even further cooling of the surface layer air, unless the inversion breaks down or overturns, which may occur because of increased wind shears or other larger-scale instabilities, perhaps also in combination with atmospheric waves (Businger, 1973).

In formulating an atmospheric boundary layer study, one needs a useful model calculation. That is, are the soil, plant, and atmospheric physics in the model functioning correctly and reliably? To achieve this goal, one needs to study the details of a model program to determine if the model results are stable and whether the results are sensible, i.e., generally consistent in comparison with observed data.

In this report, I use a computer model (see sect. 2) that scientists at the Hebrew University, Department of Soil and Water Sciences, gave to me several years ago. To test the model, I generate a time series of the surface energy budget and profiles of boundary layer wind speed, potential temperature, and specific humidity for daytime (atmospherically unstable conditions) and for nighttime (atmospherically stable conditions). I compare these model results, wherever practical, with observations from days 33 and 34 of the Wangara experiment (Clarke et al, 1971). From these results, I examine how the model characterizes transfers of momentum, heat, and moisture. I attempt to quantify these results by preparing root mean square error (rmse) and d values, where d is an index of agreement (described in sect. 5), to summarize the model comparison with observed data.

2. Model Description

The one-dimensional soil, plant, and atmospheric model used in this report has been documented previously in Pielke and Mahrer (1975), McNider and Pielke (1981), and Avissar and Mahrer (1988). It is a first-order closure model to calculate the transfer of momentum, heat, and moisture at the surface and aloft. It uses an implicit finite difference scheme to integrate the boundary layer and soil diffusion equations. It contains a complete model of the surface energy budget and a time-dependent calculation of the height of the daytime planetary boundary layer. I added the formulation suggested by Smeda (1979) for the time-dependent calculation of the height of the nighttime stable layer. The model surface layer turbulence scaling is as described by Zilitinkevich (1970) and Businger et al (1971).

As initial input, the model requires day of the year and time of day data, latitude and longitude, fraction of sky cloudiness, and ground-cover data (i.e., canopy height, leaf area index, surface reflectivity (albedo), thermal emissivity, and surface roughness). Typical values for albedo and surface roughness have been documented by Hansen (1993a, 1993b). The model computes soil properties (e.g., hydraulic and thermal conductivity and soil-specific heat capacity) from inputs of soil water content, porosity, texture (i.e., proportion of sand, clay, and organic matter), and bulk density. Other model constants include subsoil properties, such as plant root density and distribution. Also, the model requires an initial profile of wind speed, air temperature, and specific humidity (atmospheric water vapor content) from the ground level to the top of the model. Model parameters for this report are summarized in table 1.

The model equations for the time-dependent calculation of the winds (u and v components), potential temperature (θ), and specific humidity (q) over flat earth can be expressed as

$$\frac{\partial \overline{u}}{\partial t} = f\left(\overline{v} - v_g\right) + \frac{\partial}{\partial z}\left(K_m \frac{\partial \overline{u}}{\partial z}\right), \tag{1}$$

$$\frac{\partial \overline{v}}{\partial t} = f\left(u_g - \overline{u}\right) + \frac{\partial}{\partial z}\left(K_m \frac{\partial \overline{v}}{\partial z}\right), \tag{2}$$

$$\frac{\partial \overline{\theta}}{\partial t} = \frac{\partial}{\partial z}\left(K_h \frac{\partial \overline{\theta}}{\partial z}\right), \text{ and} \tag{3}$$

$$\frac{\partial \overline{q}}{\partial t} = \frac{\partial}{\partial z}\left(K_q \frac{\partial \overline{q}}{\partial z}\right), \tag{4}$$

where f denotes the Coriolis parameter (the deflecting force caused by the earth's rotation acting upon moving air), the subscript g refers to the geostrophic wind (such that the first term on the right contains the pressure gradient acceleration), K_m denotes the eddy transfer coefficient for

Table 1. Boundary layer model parameters.

Parameter	Value
Number of vertical levels	32 (2, 10, 50, 100, 150, 200, 250, 300, 350, 400, 450, 500, 550, 600, 650, 700, 750, 800, 850, 900, 950, 1000, 1100, 1200, 1300, 1400, 1500, 1600, 1700, 1800, 1900, 2000 m)
Latitude, longitude	34.50 S, 144.93 E
Surface roughness	0.0045 m
Vegetation (sparse)	0.01 m
Surface albedo	0.20
Surface emissivity	0.98
Soil water content	0.08 m^3/m^3
Average soil density	1600 kg/m^3
Soil texture (% sand, % clay, % organic)	28.0, 70.0, 2.0
Day, month, year	16–17 August 1967
Geostrophic wind (u_g, v_g)	-5.34 m/s, -0.43 m/s
Initial time	09 lt
Time step	10 s

momentum, and $K_h = K_q$ denotes the transfer coefficients for heat and moisture. In the surface layer, K_m and K_h are calculated as $K_m = \mathrm{k}u_* z/\phi_m$ and $K_h = \mathrm{k}u_* z/\phi_h$, respectively, where k is Karman's constant (= 0.4); z is height above ground level (in meters); u_* is the friction velocity (in units of m/s^{-1}), which relates to surface stress; and the ϕ_m and ϕ_h are nondimensional lapse-rate functions, which account for surface-layer stabilities other than neutral. A list of symbol definitions is provided in the appendix.

In the unstable daytime boundary layer, the model derives the transfer coefficients as a function of height, as suggested by O'Brien (1970). This function can be expressed as

$$K_z = K_{z_i} + \left(\frac{(z_i - z)^2}{(z_i - z_s)^2}\right)\left\{K_{z_s} - K_{z_i} + (z - z_s) \times \left[\frac{\partial K_{z_s}}{\partial z} + \frac{2\left(K_{z_s} - K_{z_i}\right)}{(z_i - z_s)}\right]\right\}, \tag{5}$$

where z is height above ground level and z_i and z_s refer to the heights of the top of the surface layer and top of the boundary layer, respectively. The profile function is applied similarly for the momentum, heat, and moisture coefficients. The model sets $z_s = 0.04 z_i$, $K_{z_i} = 1.0$, and $K_z = 1.0$ for $z \geq z_i$. Figure 1 illustrates the geometry (i.e., vertical levels) of the model.

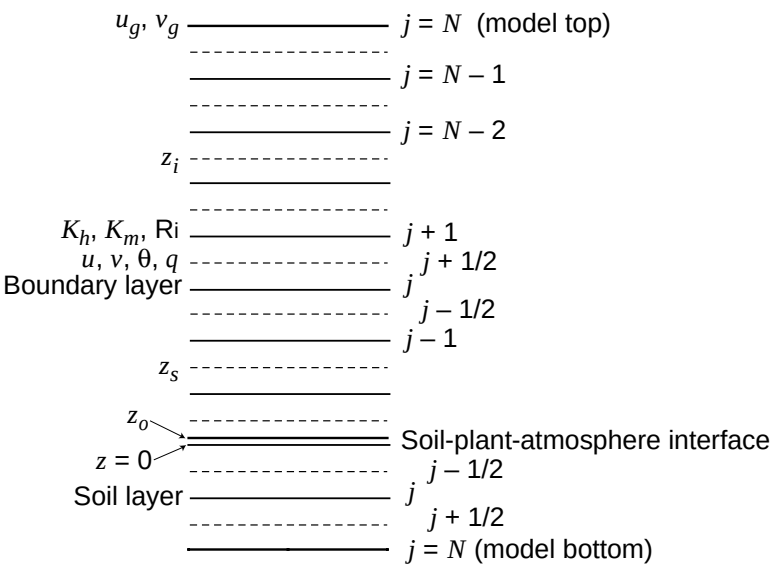

Figure 1. Sketch of geometry (i.e., vertical levels) of model.

The growth of the daytime planetary boundary layer is calculated with an expression derived by Deardorff (1974), which can be written as

$$\frac{dz_i}{dt} - w_{zi} = \frac{1.8\left(w_*^3 + 1.1u_*^3 - 3.3u_*^2 f z_i\right)}{g\left(\frac{z_i^2}{\theta_s}\right)\left(\frac{\partial\theta^+}{\partial z}\right) + 9w_*^2 + 7.2u_*^2}, \tag{6}$$

where w_{zi} is the vertical velocity at z_i (w_{zi} is assumed to be negligible or equal to zero, since time-dependent calculations of vertical velocities are not explicitly derived), $\partial\theta^+/\partial z$ is the vertical gradient of potential temperature in the stable air immediately above the boundary-layer top, θ_s is the potential temperature at the top of the surface layer z_s, and $w_* = \left[(-g/\theta)\, u_*\theta_* z_i\right]^{1/3}$ is the vertical velocity scaling variable, an implicit calculation of buoyancy, where g is acceleration caused by gravity, and $\theta_* = \frac{kz}{\phi_h}\frac{\partial\theta}{\partial z}$, the potential temperature scaling constant.

During the nighttime, when the surface layer is stable (i.e., $\theta_* > 0$), the model derives eddy transfer coefficients above the surface layer,* as suggested by Blackadar (1979), i.e.,

$$K_m(z) = K_h(z) = \begin{cases} sl^2\left(1 - 18\mathrm{Ri}\right)^{0.5}, \mathrm{Ri} < 0 \\ sl^2\left(\mathrm{Ri}_{\mathrm{crit}} - \mathrm{Ri}\right)/\mathrm{Ri}_{\mathrm{crit}}, 0 < \mathrm{Ri} \le \mathrm{Ri}_{\mathrm{crit}} \\ 0, \mathrm{Ri} > \mathrm{Ri}_{\mathrm{crit}} \end{cases}, \tag{7}$$

where s is the local wind shear, $s = \sqrt{\left(\partial u/\partial z\right)^2 + \left(\partial v/\partial z\right)^2}$, and Ri is the ratio of thermal to mechanical (wind shear) production turbulent energy called the Richardson number, so that $\mathrm{Ri} = \frac{g}{\theta}\frac{\partial\theta}{\partial z}/\left(\left(\partial u/\partial z\right)^2 + \left(\partial v/\partial z\right)^2\right)$.

*Note: $z_s = 0.15\, z_i$ while $\theta_* > 0$.

$\mathrm{Ri}_{\mathrm{crit}}$ is the limiting value of the Richardson number, and it is often assumed that $\mathrm{Ri}_{\mathrm{crit}} = 0.25$, even though $\mathrm{Ri}_{\mathrm{crit}} = 1.0$ can sometimes be a useful approximation (Avissar and Mahrer, 1988). The length l (in meters) is generally thought of as the width of turbulence and can be characterized by the formulation reported in Blackadar (1979) for $z > z_s$ as

$$l = kz \left(1 + \frac{kz}{0.0063 u_* / f} \right)^{-1}. \tag{8}$$

The height of the nighttime planetary boundary layer is calculated with the formulation suggested by Smeda (1979), which can be expressed as

$$\frac{dz_i}{dt} = 0.06 \frac{u_*^2}{z_i f} \left[1 - \left(\frac{3.3 z_i f}{u_*} \right)^3 \right]. \tag{9}$$

The surface energy budget is applied to the soil, the plant canopy and the air throughout the canopy, and the thin layer of air that extends above the canopy top (Avissar et al, 1986). Air temperature and water vapor content for each layer are derived because of energy and water vapor transfers within the system. The net radiative flux is approximated as functions of transmission, albedo, leaf area, and soil wetness. The model radiation and energy budget as described in Pielke (1984) are

$$(1 - A) R_{s\downarrow} + R_{L\downarrow} - R_{L\uparrow} - \rho c_p u_* \theta_* - \rho L_v u_* q_* + Q_s = F, \tag{10}$$

where A is surface reflectivity (albedo); $R_{s\downarrow}$, $R_{L\downarrow}$, and $R_{L\uparrow}$ are the incoming solar, incoming long-wave, and outgoing long-wave radiative fluxes, respectively; ρ is air density; c_p is the specific heat of air at constant pressure; u_*, θ_*, and q_* are the surface-layer turbulence scaling parameters for wind speed, temperature, and moisture, in that order; L_v is the heat of transformation for water vapor; Q_s is the soil heat flux; and F is the function applied in solving for the surface temperature θ_{sfc}. Using the Newton-Raphson iterative algorithm, I can approximate each successive estimate of the surface temperature as

$$\theta_{\mathrm{sfc}}{}^{(m+1)} = \theta_{\mathrm{sfc}}{}^{(m)} - \frac{F}{F'}, \tag{11}$$

where $F' = \frac{\partial F}{\partial \theta_{\mathrm{sfc}}}$.

The model equations for the soil layer and plant canopy are described in much greater detail by Avissar and Mahrer (1988), with one exception. The model formulation for downward long-wave radiation is instead based on the empirical relationship reported by Paltridge and Platt (1976), which can be expressed as

$$R_{L\downarrow} = -170.9 + 1.195\, \sigma\, T_r^4 + 0.3\, \mathrm{cld} \varepsilon_c\, \sigma T_c^4, \tag{12}$$

where $\sigma = 5.6697 \times 10^{-8}$ W/m^2 deg^{-4}, T_r is the reference level ($\sim$2 m) temperature in Kelvin, cld is the cloud amount, ε_c is the emissivity of the

cloud base, and T_c is the temperature of the cloud base in Kelvin. This formulation is much simpler to apply than computing the upward and downward long-wave radiation according to the concentrations, path lengths, and emissivities for water vapor and carbon dioxide. Also, this expression was used successfully in two previous studies (Rachele and Tunick, 1994; Tunick et al, 1994).

3. Numerical Methods and Boundary Conditions

The numerical integration of equations (1) to (4) is achieved with the use of a generalized form of the Crank-Nicholson implicit finite difference scheme (Paegle et al, 1976) to solve for the vertical transfer of momentum, heat, and moisture in the atmosphere. The diffusion terms in equations (1) to (4) can be expressed in terms of both a current τ and future $\tau + 1$ timestep:

$$\frac{\phi^{\tau+1} - \phi^{\tau}}{\Delta t} = \left[\begin{array}{l} K_{j+1/2} \frac{\beta_\tau \left(\phi^{\tau}_{j+1} - \phi^{\tau}_{j}\right) + \beta_{\tau+1} \left(\phi^{\tau+1}_{j+1} - \phi^{\tau+1}_{j}\right)}{\Delta z_{j+1/2}} \\ -K_{j-1/2} \frac{\beta_\tau \left(\phi^{\tau}_{j} - \phi^{\tau}_{j-1}\right) + \beta_{\tau+1} \left(\phi^{\tau+1}_{j} - \phi^{\tau+1}_{j-1}\right)}{\Delta z_{j-1/2}} \end{array} \right], \tag{13}$$

where $\beta_\tau + \beta_{\tau+1} = 1$, $\Delta z_j = z_{j+1/2} - z_{j-1/2}$, $\Delta z_{j+1} = z_{j+1} - z_j$, and $\Delta z_{j-1} = z_j - z_{j-1}$. In this study, $\beta_\tau = 0.75$ and $\beta_{\tau+1} = 0.25$ are the weights to the current and future contributions to the numerical approximation (Pielke, 1984). Equation (13) can be rewritten as $a_j \phi_{j-1} + b_j \phi_j + c_j \phi_{j+1} = d_j$ such that

$$\begin{aligned} &- \frac{\beta_{\tau+1} K_{j-1/2} \Delta t}{\Delta z_j \Delta z_{j-1/2}} \phi^{\tau+1}_{j-1} + \left[1 + \frac{\beta_{\tau+1} K_{j+1/2} \Delta t}{\Delta z_j \Delta z_{j+1/2}} + \frac{\beta_{\tau+1} K_{j-1/2} \Delta t}{\Delta z_j \Delta z_{j-1/2}} \right] \phi^{\tau+1}_{j} - \frac{\beta_{\tau+1} K_{j+1/2} \Delta t}{\Delta z_j \Delta z_{j+1/2}} \phi^{\tau+1}_{j+1} \\ &= \phi^{\tau}_{j} + \left[\frac{\beta_\tau K_{j+1/2} \Delta t \left(\phi^{\tau}_{j+1} - \phi^{\tau}_{j}\right)}{\Delta z_j \Delta z_{j+1/2}} + \frac{\beta_\tau K_{j-1/2} \Delta t \left(\phi^{\tau}_{j} - \phi^{\tau}_{j-1}\right)}{\Delta z_j \Delta z_{j-1/2}} \right]. \end{aligned} \tag{14}$$

The model solves equation (14) using the coefficients a_j, b_j, c_j, and d_j and the algorithm described by Ahlberg et al (1967), which can be expressed as

$$\phi_j = x_j + y_j \phi_{j+1}, \tag{15}$$

where $x_j = (d_j - a_j x_{j-1})/p_j$, $p_j = b_j + a_j y_{j-1}$, and $y_j = -c_j/p_j$, and where $x_0 = y_0 = 0$. When the pressure gradient and Coriolis accelerations in equations (1) and (2) are included, the coefficient d_j (i.e., the right-hand side of eq. (14)) becomes $d_j = d_j + f\left(\overline{v} - v_g\right)\Delta t$ and $d_j = d_j + f\left(u_g - \bar{u}\right)\Delta t$, respectively.

The boundary condition applied at the top of the model, i.e., $j = N$, for this solution is $\phi_N = 0.75\phi_{N-1} + 0.25\phi_{N-2}$, so that the variables near the top of the model are not fixed (i.e., not held to their initial values). This condition appears to behave well.

4. Days 33 and 34 Observations

The Wangara experiment data were collected over a large flat area ($\sim 60 \times 60$ km), consisting mainly of thin low bushes and desert grasses. The field study was conducted near the town of Hay, New South Wales, Australia (34.50 S, 144.93 E), during the 1967 southern hemisphere winter (Clarke et al, 1971). Five types of data were collected: (1) hourly meteorological tower measurements of wind speed, specific humidity, and temperature; (2) hourly surface measurements of the net radiative and soil heat flux; (3) measurements of wind speed and wind direction from 0 to 2 km agl obtained by hourly pibal (pilot balloon) flights; (4) measurements of pressure, temperature, and mixing ratio (weight of water vapor/weight of dry air) to a height of 2 km, taken by radiosonde (instrumented balloon sonde) flights at 3-hour intervals; and (5) reports of fractional, low, high, and total cloud cover (including cloud-type descriptors).

These data are sufficent to test the functioning of boundary layer models (e.g., Pielke and Mahrer, 1975; Yamada and Mellor, 1975; McNider and Pielke, 1981). Of the 1050 published reports (profiles), I used those data for the 27-hour period from 09 lt (local time) on 16 August 1967 to 12 lt on 17 August 1967. This time period was characterized mainly by clear skies, relatively light daytime wind speeds, dry soil, and strong surface-based convective heating. In contrast, the nighttime boundary layer winds over this time period were quite strong, and the surface layer cooled significantly.

5. Model Results

Figure 2 gives the time series of the modeled u and v components of wind speed and the time series of the total wind, $\sqrt{u^2+v^2}$, at 2 m agl, in comparison with days 33 and 34 observations. The observed wind speeds are shown as mostly overpredicted, especially through the period 12 to 18 lt. As a result, the values of the index of agreement* calculated for these data are about 50 to 60 percent (see table 2). These comparisons might have been improved if adjustments to the geostrophic wind and thermal wind (i.e., u_g, v_g, $\partial u_g/\partial z$, and $\partial v_g/\partial z$) were included in the calculation. I use $z_0 = 0.45$ cm based on modeling the surface energy budget over a barren field (Tunick et al, 1994). Several others, however, have used values of z_0 other than 0.45 cm; for example, Pielke and Mahrer (1975) used $z_0 = 0.12$ cm, as reported on p. 21 of Clarke et al (1971), and McNider and Pielke (1981) used $z_0 = 1.0$ cm, based on the recommendations of Yamada and Mellor (1975) and others that 0.12 cm was too small for use with the surface-layer flux formulations in their models.

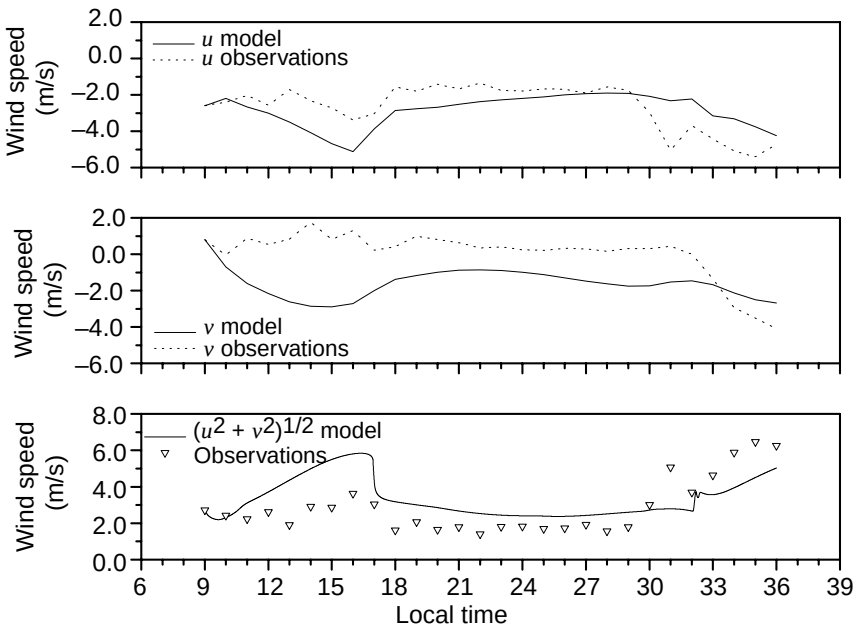

Figure 2. Modeled u and v components of wind speed and total wind, $\sqrt{u^2+v^2}$, at 2 m agl, compared with days 33 and 34 observations.

*The index of agreement d, as suggested by Willmott (1981), is calculated as

$$d = 1 - \sum_{i=1}^{n} (M_i - O_i)^2 \Big/ \sum_{i=1}^{n} \left[\left| (M_i - \bar{O}_i) \right| + \left| (O_i - \bar{O}_i) \right| \right]^2,$$

where M_i are the modeled data, O_i are the observed data, and the overbar corresponds to the mean. The nature of the index of agreement is a simple scale 0 to 100 percent, such that $d \to 1$ as the model predictions improve. In contrast, the rmse is calculated in the same units as the variable, i.e., rmse $= \left[N^{-1} \sum_{i=1}^{N} (M_i - O_i)^2 \right]^{1/2}$.

Table 2. Summary of model results in comparison with observed data.

Model parameter	rmse	d	n
Total wind speed @ 2 m agl, m/s	1.749	0.592	28
u = wind speed @ 2 m agl, m/s	1.187	0.616	28
v = wind speed @ 2 m agl, m/s	2.148	0.480	28
Temperature @ 2 m agl, K	0.627	0.966	28
Net radiative flux, W/m^2	25.098	0.995	27
Soil heat flux, W/m^2	30.273	0.955	27
Boundary layer height, m	218.495	0.888	7
Wind speed profiles, m/s (12, 15, 18, 21 lt)	2.838	0.601	120
Wind speed profiles, m/s (24, 03, 06, 09 lt)	5.010	0.372	120
Potential temperature profiles, K (12, 15, 18, 21 lt)	0.435	0.992	120
Specific humidity profiles, g/kg (12, 15, 18, 21 lt)	0.209	0.988	120

Figure 3 gives the time series of the surface and 2-m air temperatures. The modeled surface temperatures θ_{sfc} are shown in comparison with results from an earlier modeling study reported by McNider and Pielke (1981). The modeled air temperatures at 2 m, $\theta_{2\mathrm{m}}$, are shown in comparison with the days 33 and 34 observations. The results are in very good agreement with these data, especially for the daytime hours. They imply that the model's surface energy budget calculations (shown in fig. 4) are functioning properly. Index of agreement d and rmse values for these data as well as the surface energy budget are given in table 2. The discrepancies between modeled and observed data at nighttime, however, may be related to initial values of surface roughness and to certain initial soil properties, such as soil water content.

Figure 5 gives the modeled height of the planetary boundary layer. The model formulations for z_i, which are based on calculations of the surface-layer turbulence scaling parameters, appear to be in fairly good agreement, i.e., $d \approx 90$ percent, with the observations, except perhaps during the hours immediately following sunset. The observations are few because they were estimated from days 33 and 34 profiles of θ and q, taken at 3-hour intervals (see Melgarejo and Deardorff, 1974, and Pielke and Mahrer, 1975).

Figure 6 gives the modeled boundary layer wind speed profiles at 3-hour intervals in comparison with days 33 and 34 observations. During the daytime, i.e., 12 to 18 lt, the profile average wind speeds (both modeled and observed) are shown to increase through the layer $z \leq 1300$ m. Similarly, the modeled and observed profiles of wind speed at night, i.e., 24 to 06 lt, show the development of a low-level jet in the layer $100 \leq z \leq 400$ m. However, agreement between the modeled and observed profiles for these data is generally poor (i.e., $d \approx 60\%$, daytime, and $d \approx 37\%$, nighttime), particularly through the upper layers and near the model's top. From this result, I suspect that either the upper boundary condition for equations (1) and (2)

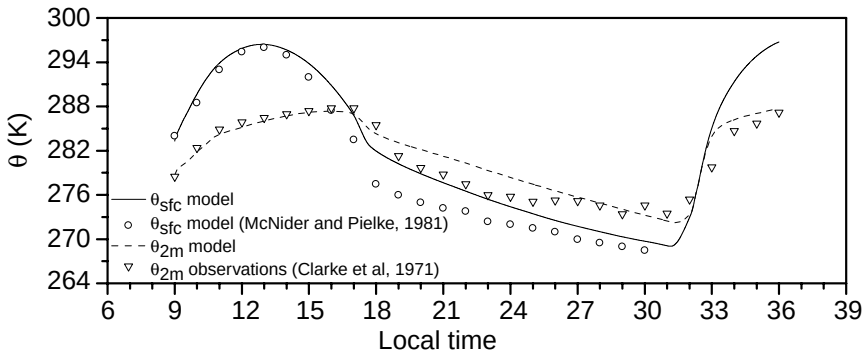

Figure 3. Modeled surface ($\theta_{\rm sfc}$) temperatures compared with results from an earlier modeling study reported by McNider and Pielke (1981) and modeled 2-m ($\theta_{\rm 2m}$) air temperatures compared with days 33 and 34 observations.

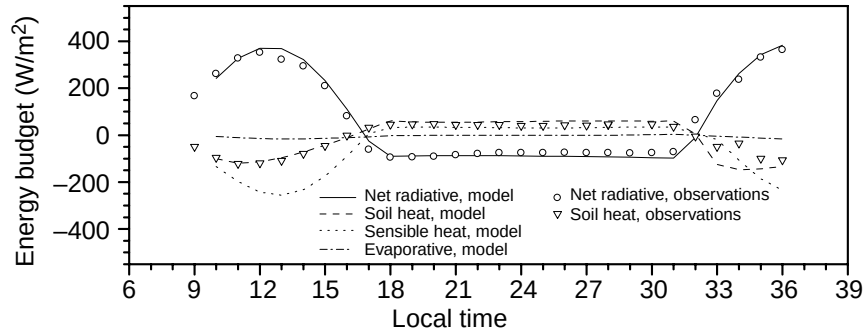

Figure 4. Modeled surface energy budget compared with days 33 and 34 observations of net radiative and soil heat flux.

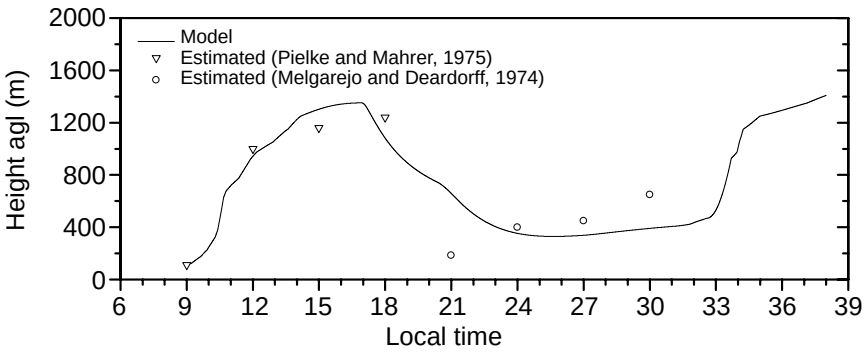

Figure 5. Modeled height of planetary boundary layer compared with days 33 and 34 observations.

does not apply and/or the observed profile data reflect changes (over time) in the geostrophic wind (see table 3), an effect that was not included in the calculation. This can be addressed in a separate study.

Figure 7 gives the modeled potential temperature and specific humidity profiles at 3-hour intervals in comparison with days 33 and 34 observations. The potential temperature profiles are well mixed vertically through the convective layer, $z \leq 1300$ m, increasing (on the average) over the daytime hours. The specific humidity profiles are also well mixed through the convective layer and are decreasing (on the average) over the daytime hours. The index of agreement between these modeled and observed data is $d \approx 0.99$. In part, this high value of agreement is because there is little or no advection of heat or moisture over time in the upper model layers. For layer $z \leq z_i$, I can infer that the eddy transfer (eddy diffusion) coefficients used in the model are formulated reasonably well. Figure 8 summarizes these comparisons of the modeled results to observed data.

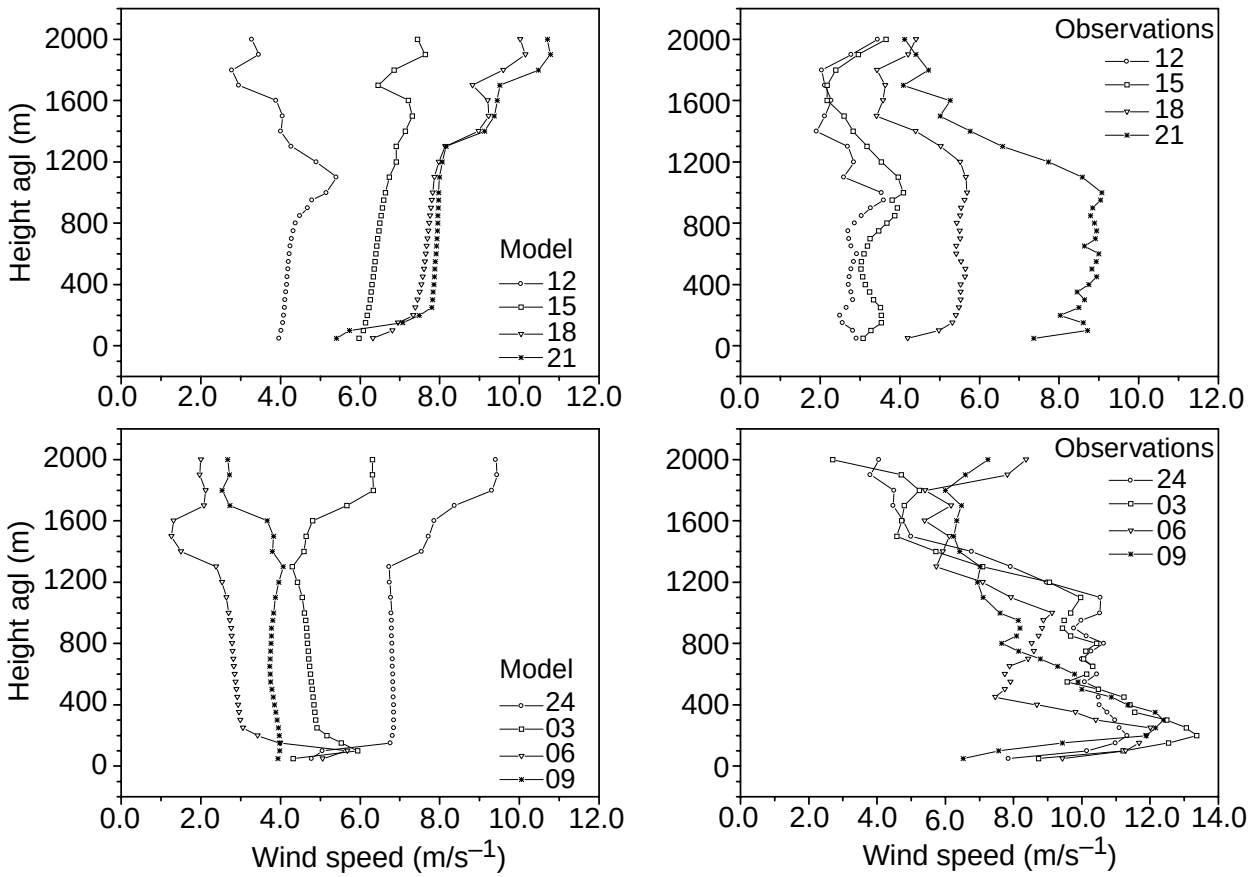

Figure 6. Model boundary layer wind speed profiles at 3-hour intervals compared with days 33 and 34 observations.

Table 3. Days 33 and 34 geostrophic wind data.

Local time	u_g (m/s)	v_g (m/s)	Total wind (m/s)	Direction (°)
09	−5.34	−0.43	5.36	85.4
12	−5.56	1.27	5.70	102.9
15	−6.20	0.98	6.28	99.0
18	−6.42	−0.72	6.46	83.6
21	−5.99	−1.93	6.29	72.1
24	−6.93	−2.86	7.50	67.6
03 (27)	−8.02	−3.13	8.61	68.9
06 (30)	−7.32	−4.97	8.85	55.8
09 (33)	−7.60	−4.72	8.95	58.2
12 (36)	−7.95	−3.43	8.66	66.7

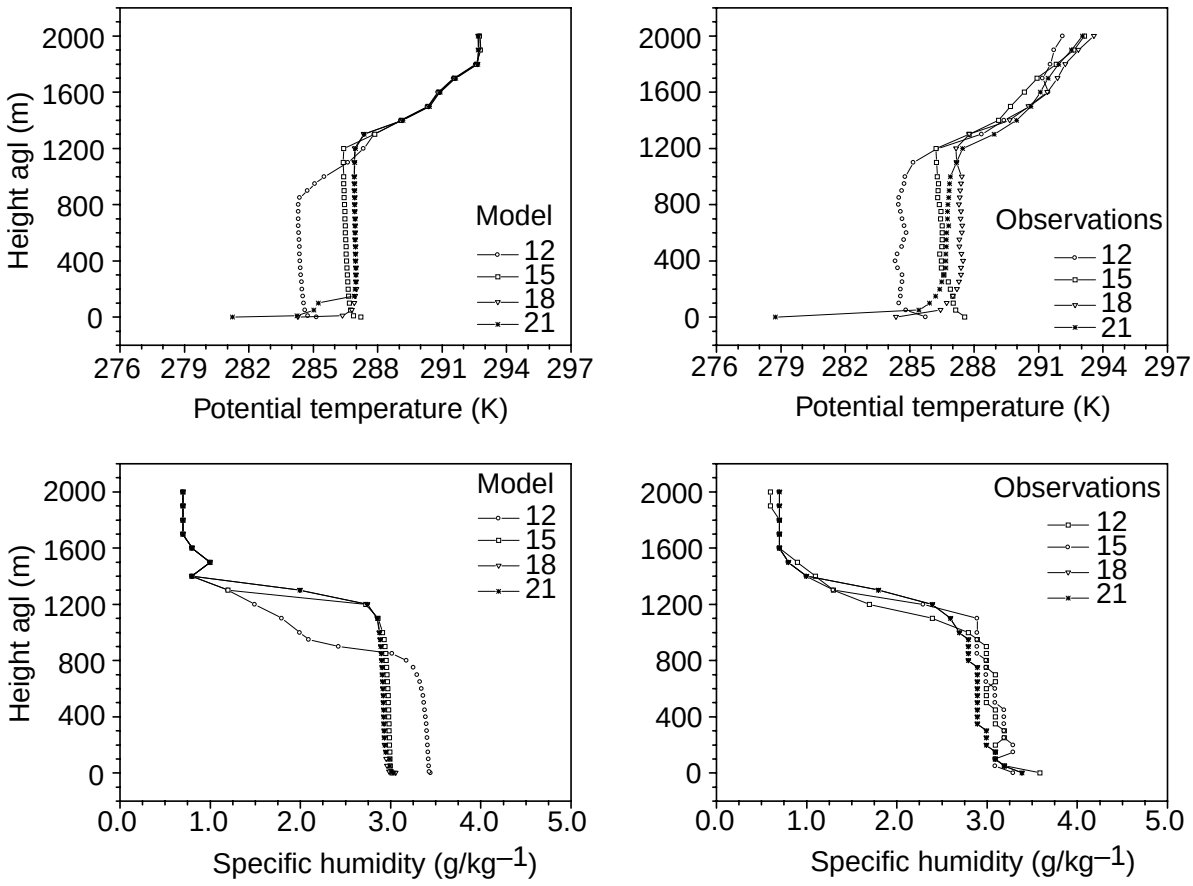

Figure 7. Modeled potential temperature and specific humidity profiles at 3-hour intervals compared with days 33 and 34 observations.

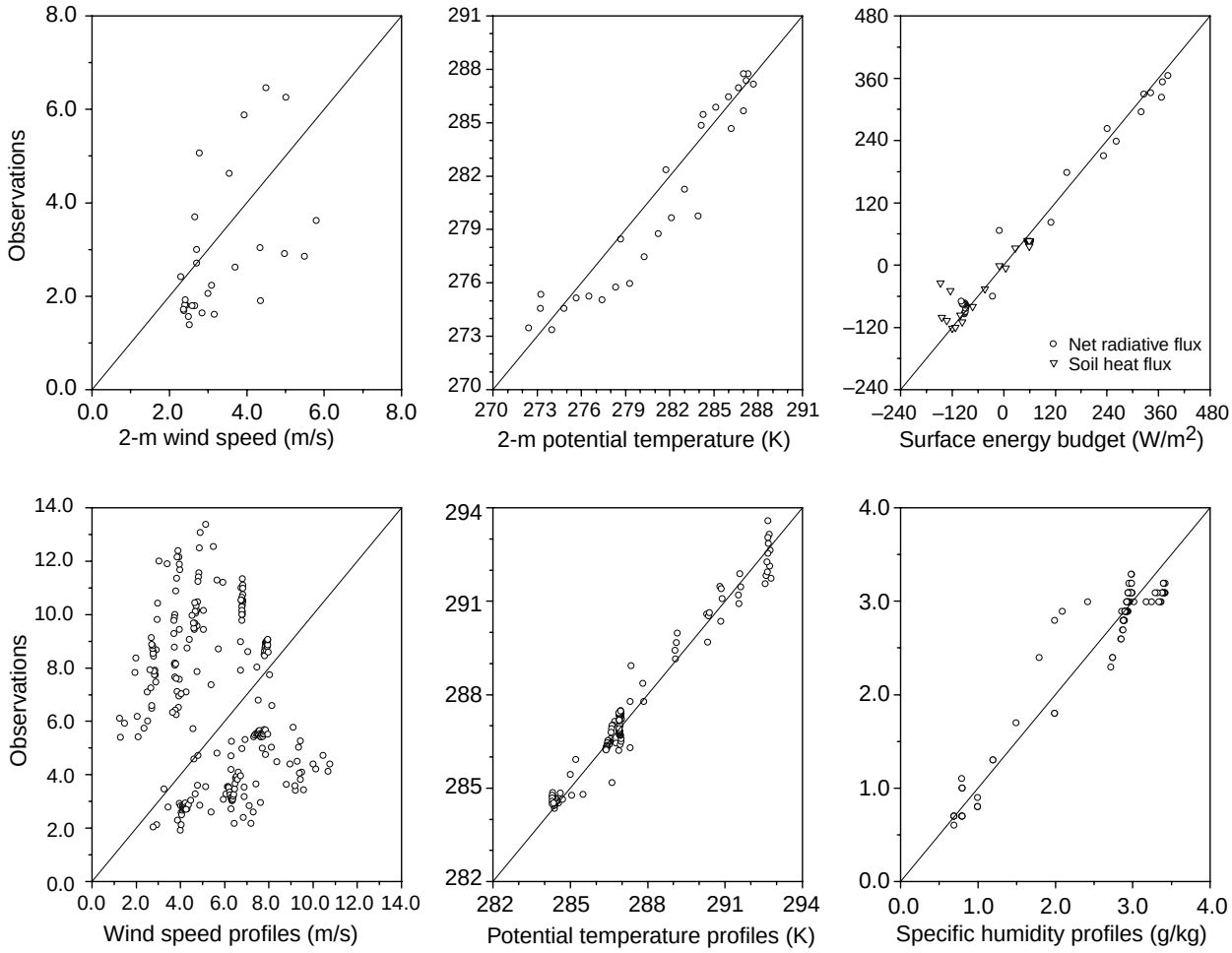

Figure 8. Scatter plot comparisons of modeled results to observed data.

6. Conclusion

For this report, I studied and modified an atmospheric boundary layer computer program. I ran the computer program, making changes to various sets of initial conditions. From this effort, I found that the one-dimensional model functions correctly and appears to be as reliable as any of the earlier models of this type (e.g., Pielke and Mahrer (1975) and McNider and Pielke (1981)) in predicting the general features of boundary layer development. I hope to use this work toward conducting an additional study on boundary layer wind shears under nighttime stable conditions.

I found this work to be very challenging. In particular, rendering the Ahlberg et al (1967) algorithm from the computer code provided a good introduction to numerical methods used in computer models.

Acknowledgments

I would like to thank Jonathan Fine, David Gerstman, Teizi Henmi, Sam Chang, and Jeffrey Passner of the U.S. Army Research Laboratory for reading though my report and offering many helpful comments. I would also like to acknowledge Ronald Meyers, Keith Deacon, and David Rosen of the U.S. Army Research Laboratory for their support and encouragement during this study.

References

1. Ahlberg, J. H., E. N. Nilson, and J. L. Walsh (1967), *The Theory of Splines and Their Applications*, Academic Press, New York, 284.

2. Avissar, R., and Y. Mahrer (1988), "Mapping frost-sensitive areas with a three-dimensional local-scale numerical model, Part I: Physical and numerical aspects," *J. Appl. Meteorol.* **27**, 400–413.

3. Avissar, R., N. Dagan, and Y. Mahrer (1986), "Evaluation, in real time, of the actual evapotranspiration using a numerical model," *Proc. Agrotics 86, Automation and Robots for Agriculture*, Bordeaux, France (18–20 March).

4. Blackadar, A. K. (1979), "High resolution models of the planetary boundary layer," *Advances in Environmental Science and Engineering* **1**, J. Pfafflin and E. Ziegler, eds., Gordon and Breach, 50–85.

5. Businger, J. A. (1973), "Turbulent transfer in the atmospheric surface layer," in *Workshop on Micrometeorology*, D. A. Haugen, ed., *Am. Meteorol. Soc.*, Boston, MA, 67–98.

6. Businger, J. A., J. C. Wyngaard, Y. Izumi, and E. F. Bradley (1971), "Flux-profile relationships in the atmospheric surface layer," *J. Atmos. Sci.* **28**, 181–189.

7. Clarke, R. H., A. J. Dyer, R. R. Brook, D. G. Reid, and A. J. Troup (1971), *The Wangara Experiment: Boundary Layer Data*, Commonwealth Scientific and Industrial Research Organization, Australia, 316.

8. Deardorff, J. W. (1974), "Three-dimensional numerical study of the height and mean structure of a heated planetary boundary layer," *Boundary Layer Meteorol.* **7**, 81–106.

9. Huschke, R. E., ed. (1959), "Glossary of Meteorology," *Am. Meteorol. Soc.*, 638.

10. Hansen, F. V. (1993a), *Albedos*, U.S. Army Research Laboratory, ARL-TR-57.

11. Hansen, F. V. (1993b), *Surface Roughness Lengths*, U.S. Army Research Laboratory, ARL-TR-61.

12. Melgarejo, J. W., and J. W. Deardorff (1974), "Stability functions for the boundary layer resistance laws based upon observed boundary layer heights," *J. Atmos. Sci.* **31**, 1324–1333.

13. McNider, R. T., and R. A. Pielke (1981), "Diurnal boundary-layer development over sloping terrain," *J. Atmos. Sci.* **38**, 2198–2212.

14. O'Brien, J. J. (1970), "A note on the vertical structure of the eddy exchange coefficient in the planetary boundary layer," *J. Atmos. Sci.* **27**, 1213–1215.

15. Paegle, J., W. G. Zdunkowski, and R. M. Welch (1976), "Implicit differencing of predictive equations of the boundary layer," *Mon. Weather Rev.* **104**, 1321–1324.

16. Paltridge, G. W., and C.M.R. Platt (1976), *Radiative Processes in Meteorology and Climatology*, Elsevier, 318.

17. Pielke, R. A. (1984), *Mesoscale Meteorological Modeling*, Academic Press, 612.

18. Pielke, R. A., and Y. Mahrer (1975), "Representation of the heated planetary boundary layer in mesoscale models with coarse vertical resolution," *J. Atmos. Sci.* **32**, 2288–2308.

19. Rachele, H., and A. Tunick (1994), "Energy balance model for imagery and electromagnetic propagation," *J. Appl. Meteorol.* **33**, 964–976.

20. Smeda, M. S. (1979), "Incorporation of planetary boundary layer process into numerical forecast models," *Boundary-Layer Meteorol.* **16**, 115-129.

21. Tunick, A., H. Rachele, F. V. Hansen, J. A. Howell, J. L. Steiner, A. D. Schneider, and S. R. Evett (1994), "REBAL '92—A cooperative radiation and energy balance field study for imagery and E. M. propagation," *Bull. Am. Meteorol. Soc.* **75**, 421–430.

22. Willmott, C. J. (1981), "On the validation of models," *Phys. Geog.* **2**, 184–194.

23. Yamada, T., and G. L. Mellor (1975), "A simulation of the Wangara atmospheric boundary layer data," *J. Atmos. Sci.* **32**, 2309–2329.

24. Zilitinkevich, S. (1970), "Dynamics of the atmospheric boundary layer," *Hydrometeorol.*, Leningrad, 291.

Appendix—Symbols and Definitions

a_j: coefficient of finite difference scheme

A: surface reflectivity (albedo)

b_j: coefficient of finite difference scheme

cld: cloud amount (in tenths)

c_j: coefficient of finite difference scheme

c_p: specific heat of air at constant pressure

d: index of agreement

d_j: coefficient of finite difference scheme

f: Coriolis parameter

F: function applied in solving for surface temperature through surface energy budget

g: acceleration caused by gravity

j: vertical level of model

k: Karman's constant (= 0.4)

K_h: eddy transfer coefficient for heat

K_m: eddy transfer coefficient for momentum

K_q: eddy transfer coefficient for moisture

l: mixing length

L_v: heat of transformation for water vapor

m: total number of iteration steps to solve for equation (10)

M_i: modeled data

n: total number of model or observed data points

N: total number of vertical grid points

O_i: observed data

p_j: coefficient in algorithm to solve for equation (14)

q: specific humidity

q_*: surface-layer turbulence scaling parameter for moisture

Q_s: soil heat flux

Ri: ratio of thermal to mechanical (wind shear) production turbulent energy called Richardson number

$\mathrm{Ri}_{\mathrm{crit}}$: limiting value of Richardson number

$R_{s\downarrow}$: incoming solar radiative flux

$R_{L\downarrow}$: incoming long-wave radiative flux

$R_{L\uparrow}$: outgoing long-wave radiative flux

s: local wind shear, $s = \sqrt{(\partial u/\partial z)^2 + \partial v/\partial z^2}$

t: time

T_c: temperature of cloud base (in Kelvin)

T_r: reference level ($\sim$2 m) temperature (in Kelvin)

u: east-west component of horizontal wind speed

u_g: east-west component of geostrophic wind speed

u_*: surface friction velocity

v: north-south component of horizontal wind speed

v_g: north-south component of geostrophic wind speed

w_{zi}: vertical velocity at z_i

W_*: vertical velocity scaling variable

x_j: coefficients in algorithm in equation (15)

y_j: coefficients in algorithm in equation (15)

z: height above ground level (agl)

z_i: height of top of planetary boundary layer

z_s: height of top of surface layer

β_τ: weighting function related to current timestep

$\beta_{\tau+1}$: weighting function related to future timestep

ϵ_c: emissivity of cloud base

ϕ_h: nondimensional temperature lapse rate

ϕ_m: nondimensional wind shear

ϕ_N: any profile variables (i.e., u, v, θ, or q)

θ: potential temperature

θ_*: potential temperature scaling constant

θ_{sfc}: surface potential temperature

$\theta_{2\mathrm{m}}$: potential temperature at 2 m

ρ: air density

σ: Stefan-Boltzmann constant

τ: indicates current timestep

$\tau + 1$: indicates future timestep

$\overline{\mathrm{any}}$: overbar denotes the mean

Distribution

Admnstr
Defns Techl Info Ctr
Attn DTIC-OCP
8725 John J Kingman Rd Ste 0944
FT Belvoir VA 22060-6218

Mil Asst for Env Sci Ofc of the Undersec of
Defns for Rsrch & Engrg R&AT E LS
Pentagon Rm 3D129
Washington DC 20301-3080

ARL Chemical Biology Nuc Effects Div
Attn AMSRL-SL-CO
Aberdeen Proving Ground MD 21005-5423

Army Corps of Engrs Engr Topographics Lab
Attn CETEC-TR-G P F Krause
7701 Telegraph Rd
Alexandria VA 22315-3864

Army Field Artillery School
Attn ATSF-TSM-TA
FT Sill OK 73503-5000

Army Infantry
Attn ATSH-CD-CS-OR E Dutoit
FT Benning GA 30905-5090

Army Materiel Sys Analysis Activity
Attn AMXSY-CS Bradley
Aberdeen Proving Ground MD 21005-5071

Army TACOM-ARDEC
Attn AMSTA-AR-WEL-TL
Bldg 59 Phillips Rd
Picatinny Arsenal NJ 07806-5000

Kwajalein Missile Range
Attn Meteorologist in Charge
PO Box 57
APO San Francisco CA 96555

Natl Ground Intllgnc Ctr
Army Foreign Sci Tech Ctr
Attn CM
220 7th Stret NE
Charlottesville VA 22901-5396

Natl Security Agency
Attn W21 Longbothum
9800 Savage Rd
FT George G Meade MD 20755-6000

Pac Mis Test Ctr Geophysics Div
Attn Code 3250 Battalino
Point Mugu CA 93042-5000

Science & Technology
101 Research Dr
Hampton VA 23666-1340

SMC/CZA
2435 Vela Way Ste 1613
El Segundo CA 90245-5500

US Army Aviation and Missile Command
Attn AMSMI-RD-WS-PL G Lill Jr
Bldg 7804
Redstone Arsenal AL 35898-5000

US Army Combined Arms Combat
Attn ATZL-CAW
FT Leavenworth KS 66027-5300

US Army CRREL
Attn CRREL-GP R Detsch
Attn CRREL-RG Boyne
72 Lyme Rd
Hanover NH 03755-1290

US Army Dugway Proving Ground
Attn STEDP 3
Attn STEDP-MT-DA-L-3
Attn STEDP-MT-M Biltoft
Attn STEDP-MT-M Bowers
Dugway UT 84022-5000

US Army OEC
Attn CSTE-AEC-FSE
4501 Ford Ave Park Center IV
Alexandria VA 22302-1458

US Army Spc Technology Rsrch Ofc
Attn Brathwaite
5321 Riggs Rd
Gaithersburg MD 20882

Distribution (cont'd)

US Army Topo Engrg Ctr
Attn CETEC-ZC
FT Belvoir VA 22060-5546

US Army TRADOC Anlys Cmnd—WSMR
Attn ATRC-WSS-R
White Sands Missile Range NM 88002

US Army White Sands Missile Range
Attn STEWS-IM-ITZ Techl Lib Br
White Sands Missile Range NM 88002-5501

US Military Academy
Mathematical Sci Ctr of Excellence
Attn MADN-MATH MAJ R Huber
Thayer Hall
West Point NY 10996-1786

USATRADOC
Attn ATCD-FA
FT Monroe VA 23651-5170

Nav Air War Cen Wpn Div
Attn CMD 420000D C0245 A Shlanta
1 Admin Cir
China Lake CA 93555-6001

Nav Rsrch Lab
Attn Code 4110 Ruhnke
Washington DC 20375-5000

Naval Surface Weapons Ctr
Attn Code G63
Dahlgren VA 22448-5000

AFCCC/DOC
Attn Glauber
Attn Weather Techl Lib
151 Patton Ave Rm 120
Asheville NC 28801-5002

Directed Energy Directorate
Attn AFRL/DEBA
3550 Aberdeen Ave SE
Kirtland AFB NM 87117-5776

Hdqtrs AFWA/DNX
106 Peacekeeper Dr Ste 2N3
Offutt AFB NE 68113-4039

Phillips Lab Atmos Sci Div
Geophysics Dirctrt
Attn McClatchey
Hanscom AFB MA 01731-5000

Phillips Lab Atmospheric Sci Div
Geophysics Dirctrt
Attn PL-LYP Chisholm
Kirtland AFB NM 87118-6008

PL/WE
Kirtland AFB NM 87118-6008

TAC/DOWP
Langley AFB VA 23665-5524

USAF Rome Lab Tech
Attn Corridor W Ste 262 RL SUL
26 Electr Pkwy Bldg 106
Griffiss AFB NY 13441-4514

NASA Marshal Spc Flt Ctr Atmos Sci Div
Attn Code ED 41 1
Attn Code ED-41
Huntsville AL 35812

Colorado State Univ Dept of Atmos Sci
Attn R A Pielke
FT Collins CO 80523

Cornell Univ School of Civil & Env
Attn W H Brutsaert
Hollister Hall
Ithica NY 14853-3501

Florida State Univ
Dept of Meteorology
Attn E A Smith
Tallahassee FL 32306

Iowa State Univ
Attn E S Takle
Attn R Arritt
312 Curtiss Hall
Ames IA 50011

Distribution (cont'd)

Iowa State Univ
Attn M Segal
Attn S E Taylor
2104 Agronomy Hall
Ames IA 50011-1010

Michigan State Univ
Dept of Crop & Soil Sci
Attn J Ritchie
8570 Plant & Soil Sciences Bldg
East Lansing MI 48824-1325

Penn State Univ
Dept of Meteorology
Attn D Thompsom
503 Walker Bldg
University Park PA 16802

Rutgers Univ-Cook Campus Envir & Natl Resources Bldg
Attn R Avissar
New Brunswick NJ 08903

The City College of New York
Dept of Earth & Atmos Sci
Attn S D Gedzelman
J106 Marshak Bldg 137th and Covent Ave
New York City NY 10031

Univ of Alabama at Huntsville Rsrch Inst
Attn R T Mcnider
Huntsville AL 35899

Univ of California at Davis
Dept of Air, Land, & Water Resources
Attn R H Shaw
Davis CA 95616

Univ of Connecticut
Dept of Renewable Natural Resources
Attn D R Miller
1376 Storrs Rd
Storrs CT 06269-4087

Univ of Kansas
Dept of Physics & Astronomy
Attn J R Eagleman
Lawrence KS 66045

Univ of Nebraska
Dept of Agrcltl Meteorology
Attn S B Verma
Lincoln NE 68583-0728

Washington State Univ
Dept of Agronomy & Soils
Attn G S Campbell
Pullman WA 99163

Agrclt Rsrch Svc Conserve & Prodn Rsrch Lab
Attn A D Schneider
Attn S R Evett
Attn T A Howell
PO Drawer 10
Bushland TX 79012

Dean RMD
Attn Gomez
Washington DC 20314

Dept of Commerce Ctr
Mountain Administration
Attn Spprt Ctr Library R51
325 S Broadway
Boulder CO 80303

Natl Ctr for Atmospheric Research
Attn NCAR Library Serials
PO Box 3000
Boulder CO 80307-3000

NCAR
Attn T W Horst
PO Box 3000
Boulder CO 80307-3000

NCAR/SSSF
Attn S P Oncley
PO Box 3000
Boulder CO 80307-3000

NCSU
Attn J Davis
PO Box 8208
Raleigh NC 27650-8208

Distribution (cont'd)

USDA Agrcltl Rsrch Svc
Attn W P Kustas
BARCOWEST Bldg 265
Beltsville MD 20705

USDA Agrcltl Rsrch Svc
Attn S B Idso
Attn S Moran
4331 E Broadway Rd
Phoenix AZ 85040

USDA Forest Svc
Rocky Mtn Frst & Range Exprmnt Sta
Attn K F Zeller
240 W Prospect Stret
FT Collins CO 80526

US Army Rsrch Lab
Attn AMSRL-CI-EW
Attn AMSRL-CI-EA
Battlefield Envir Div
White Sands Missile Range NM 88002-5001

US Army Rsrch Ofc
Attn AMSRL-RO-EN W D Bach
PO Box 12211
Research Triangle Park NC 27709

US Army Rsrch Lab
Attn AMSRL-DD J Miller
Attn AMSRL-CI-AI-R Mail & Records Mgmt
Attn AMSRL-CI-AP Techl Pub (3 copies)
Attn AMSRL-CI-LL Techl Lib (3 copies)
Attn AMSRL-CI J D Gantt
Attn AMSRL-CI-E
Attn AMSRL-CI-EP
Attn AMSRL-CI-EM
Attn AMSRL-CI-EP A D Tunick (16 copies)
Attn AMSRL-CI-EB R Meyers
Adelphi MD 20783-1197

REPORT DOCUMENTATION PAGE

Form Approved
OMB No. 0704-0188

1. AGENCY USE ONLY *(Leave blank)*	2. REPORT DATE	3. REPORT TYPE AND DATES COVERED
	September 2000	Final, January to May 2000

4. TITLE AND SUBTITLE A One-Dimensional Atmospheric Boundary Layer Model: Comparison with Observations

5. FUNDING NUMBERS
DA PR: B53A
PE: 61102A

6. AUTHOR(S) Arnold Tunick

7. PERFORMING ORGANIZATION NAME(S) AND ADDRESS(ES)
U.S. Army Research Laboratory
Attn: AMSRL-CI-EP email: atunick@arl.army.mil
2800 Powder Mill Road
Adelphi, MD 20783-1197

8. PERFORMING ORGANIZATION REPORT NUMBER
ARL-MR-484

9. SPONSORING/MONITORING AGENCY NAME(S) AND ADDRESS(ES)
U.S. Army Research Laboratory
2800 Powder Mill Road
Adelphi, MD 20783-1197

10. SPONSORING/MONITORING AGENCY REPORT NUMBER

11. SUPPLEMENTARY NOTES
ARL PR: 9FEJ70
AMS code: 611102.53A

12a. DISTRIBUTION/AVAILABILITY STATEMENT Approved for public release; distribution unlimited.

12b. DISTRIBUTION CODE

13. ABSTRACT *(Maximum 200 words)*

This report examines details of a one-dimensional (1D) atmospheric boundary layer model to establish the proper functioning of its soil, plant, and atmospheric physics. To achieve this goal, I inspect, repair, and modify a computer program that scientists at the Hebrew University, Department of Soil and Water Sciences, gave to me years ago. The computer program was exercised to determine if the model results are stable when initial conditions are changed and to determine whether the results are sensible and generally consistent with observed data. To show this, I present a time series of the modeled surface energy budget and modeled profiles of boundary layer wind speed, potential temperature, and specific humidity for daytime (atmospherically unstable conditions) and for nighttime (atmospherically stable conditions). I compare these results, wherever practical, with observed meteorological data. From these results, I infer how well the transfers of momentum, heat, and moisture from one model layer to the next are characterized. I also present root mean square error and *d* values, where *d* is an index of agreement, to summarize the model results and comparison with observed data. From the results, I find that the 1D model is functioning properly in solving for many parameter relationships and is as reliable as the earlier models of this type in predicting the general features of boundary layer development.

14. SUBJECT TERMS Model validation, soil physics, plant physics, low-level jet, meteorology temperature inversion, geostrophic wind

15. NUMBER OF PAGES
31

16. PRICE CODE

17. SECURITY CLASSIFICATION OF REPORT	18. SECURITY CLASSIFICATION OF THIS PAGE	19. SECURITY CLASSIFICATION OF ABSTRACT	20. LIMITATION OF ABSTRACT
Unclassified	Unclassified	Unclassified	UL

NSN 7540-01-280-5500

Standard Form 298 (Rev. 2-89)
Prescribed by ANSI Std. Z39-18
298-102